Spacetime-emergent ring toward tabletop quantum gravity experiments

Koji Hashimoto,* Daichi Takeda,† Koichiro Tanaka,‡ and Shingo Yonezawa§
Department of Physics, Kyoto University, Kyoto 606-8502, Japan

(Received 13 January 2023; accepted 10 April 2023; published 16 June 2023)

We propose a way to discover, in tabletop experiments, spacetime-emergent materials, that is, materials holographically dual to higher-dimensional quantum gravity systems under the AdS/CFT. The emergence of the holographic spacetime is verified by a mathematical imaging transform of the response function on the material. We consider theories on a one-dimensional ring-shaped material and compute the response to a scalar source locally put at a point on the ring. When the theory on the material has a gravity dual, the imaging in the low-temperature phase exhibits a distinct difference from the ordinary materials: The spacetime-emergent material can look into the holographically emergent higher-dimensional curved spacetime and provides an image as if a wave had propagated there. Therefore the image is an experimental signature of the spacetime emergence. We also estimate the temperature, ring size, and source frequency usable in experiments, with an example of a quantum critical material, $TlCuCl_3$.

DOI: 10.1103/PhysRevResearch.5.023168

I. INTRODUCTION

In contrast to the variety of theoretical scenarios considered so far, quantum gravity has not yet been tested experimentally. There are two major directions for quantum gravity experiments: direct measurement of quantum gravity corrections in our universe, and studying materials as emergent gravity systems. Since the former approach requires energy around the Planck scale, which is a severe obstacle, it is reasonable to pioneer the latter possibility, tabletop experiments for quantum emergent gravity.

Holography, the anti–de Sitter and conformal field theory (AdS/CFT) correspondence [1], offers the progress for that. Nonholographic examples of materials which exhibit effective gravitational phenomena include acoustic black holes [2] and type II topological material [3], while holography is rather an established framework which can provide a duality to truly quantum gravity, not just to the classical part of the gravity or just curved spacetimes. In this paper, to build a foundation for quantum gravity tests, we propose a way to discover ring-shaped *spacetime-emergent materials* (SEMs), materials equivalent to higher-dimensional quantum gravity systems under the AdS_3/CFT_2 correspondence [4]. We demonstrate theoretical calculations of the response function on the ring, and find that optical imaging transformation, which is performed mathematically, helps discriminate materials letting three-dimensional gravity spacetimes be emergent holographically. That is, we claim that, by imaging the response signal on the ring, SEMs can be discovered in laboratory tabletop experiments. The discovery of an SEM leads directly to the quantum gravity tests, as it amounts to a technology to create our own universe of micro- or nanoscale size, which is the playground for the experimental study of Hawking radiation, the information loss problem of black holes, and even the birth of the universe.

In the remainder of this section, we will position our work, following the history of the AdS/CFT correspondence in a way friendly to readers who are not familiar with holography.

Conformal field theory (CFT) is a nongravitational relativistic quantum field theory which has conformal symmetry (and thus is scale-free), and anti-de Sitter (AdS) spacetime is a maximally symmetric spacetime which solves the Einstein equation with a negative cosmological constant. The AdS/CFT correspondence, dubbed the holographic duality, claims that a certain CFT is equivalent to some higher-dimensional system containing gravitational degrees of freedom on the AdS spacetime background. Given that such a CFT_d is defined on a $(d-1)$-dimensional sphere $\mathbb{S}^{d-1}$ (which is a compact space with a unique scale, the radius of the sphere [5]), then the dual gravity theory is to be defined inside the sphere with the time coordinate shared, the AdS_{d+1} spacetime (see Fig. 1). Hence where the CFT is defined is called the boundary, and the AdS side is the bulk. As this duality originates in string theory, the quantum nature of the gravity is already a part of the formulation, and especially the bulk Planck scale is not necessarily so large as that of our universe. This is why it is important to find materials following the AdS/CFT correspondence.

Since, at zero temperature, CFT is scale-free unless compactified, it is expected that, near quantum critical points, there could be materials well approximated by some CFTs. Thus the AdS/CFT correspondence suggests the existence

*koji@scphys.kyoto-u.ac.jp
†takedai@gauge.scphys.kyoto-u.ac.jp
‡kochan@scphys.kyoto-u.ac.jp
§yonezawa.shingo.3m@kyoto-u.ac.jp

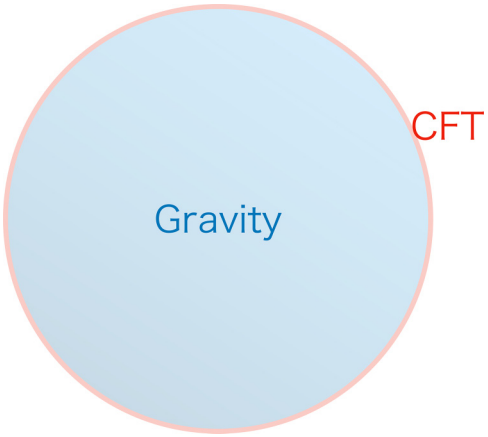

FIG. 1. Illustration of the AdS/CFT correspondence. The bulk spacetime hosts a gravity system, while the boundary spacetime hosts the material CFT. The CFT is equivalent to the gravity. The time coordinate is not depicted here.

of SEMs. Studies related to this are called AdS–condensed matter physics (AdS/CMP) correspondence studies [6]. In this field so far, a variety of gravity models that mimic phase diagrams of some forms of condensed matter have been built, for example, as one of the most successful stories, the holographic superconductor [7,8]. However, just by examining aspects universal among certain materials, one cannot conclude for which material among them a spacetime is emergent, and what kind of spacetime emerges [9]. Is there any reasonable method which can judge whether a material that we bring to a laboratory is an SEM or not?

In the AdS/CFT correspondence, a black hole can appear in the bulk when the boundary material is at nonzero temperature. It was shown theoretically in Refs. [10,11] that a visual image of holographic black holes can be read from observables of SEMs (see also Refs. [12,13]). Here a *holographic black hole* means a black hole virtually appearing in the emergent spacetime. In the papers, the Einstein ring of the Schwarzschild-AdS$_4$ black hole was visualized, just as in our universe the image of the supermassive black hole in M87 was observed by the Event Horizon Telescope. Since the photographs of the Einstein rings are naturally interpreted as being a result of an optical wave which had propagated in the emergent curved spacetime, the imaging of holographic black holes can directly catch the spacetime emergence. Along with this novel possibility of detection of the spacetime emergence, we make a further step for realistic experiments: spacetime-emergent rings. In fact, we notice that, so long as we deal with AdS$_4$/CFT$_3$ correspondence in which the material shape is a two-dimensional sphere $\mathbb{S}^2$, we cannot apply the strategy to real experiments, because it is in general technically difficult to process a quantum material into a stable sphere. Thus in this paper we propose to use $\mathbb{S}^1$ instead: ring-shaped materials, which are relatively easy to make in laboratories. With one dimension lowered, the correspondence is now AdS$_3$/CFT$_2$.

We will also consider the well-known gravitational phase transition between the black hole phase (high temperature) and the AdS soliton phase (low temperature). In the transition the bulk geometry changes from the one with a black hole

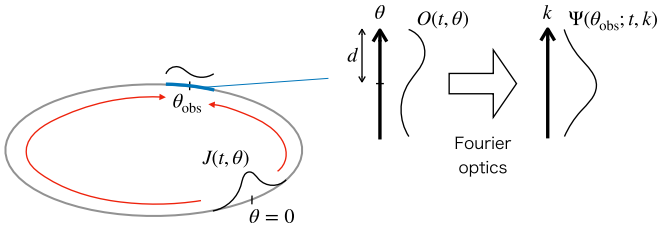

FIG. 2. The setup and strategy.

to the one without but with an energy gap. This corresponds to the conductor-insulator transition of the boundary CFT in the context of the AdS/CMP correspondence [14]. There are mainly two reasons for us to deal with the transition. First, since we are planning to realize experiments, to spot a candidate material we need to compare the transition with the one for the material. The second reason, which is more critical, is that for the case of the SEM ring the bulk of the high-temperature phase is not probed well by the imaging. All the bulk light rays shot from the boundary are absorbed by the Bañados-Teitelboim-Zanelli (BTZ) black hole (the holographic black hole in AdS$_3$) and never come back to the boundary again, meaning that the bulk information is lost. Therefore, as proven in Ref. [10], the straightforward application of the imaging strategy to the BTZ black hole fails. On the other hand, we will later find that the image in the AdS soliton phase (the low-temperature phase) is so bright only at the antipodal point of the source location, while not when we observe it at other points on the ring. This characteristic signal of the image of the response is the sign of the emergent spacetime: When we discover in experiments a material whose image has this characteristic, we can claim that the material is an SEM [15]. To clarify the universality of the feature of the signal, we also compare the result with that of a non-SEM theory, i.e., a model of materials which does not give any dual gravity.

The organization of this paper is as follows. In Sec. II, we introduce the setup and our strategy more in detail, but in a way friendly to people who are not familiar with or not interested in technical aspects of holography. In Sec. III, the response function of an ordinary material (non-SEM) and that of an SEM are computed. The results are mathematically processed by the imaging method and shown in Sec. IV. In Sec. V, proposing TlCuCl$_3$ as a candidate, we estimate parameters needed to judge in experiments whether it is an SEM. Section VI is devoted to a summary and discussion.

II. SETUP AND STRATEGY

Our proposal to judge whether a ring-shaped material is an SEM is as follows (see Fig. 2). Let t denote the time coordinate and θ denote the coordinate along the ring with the periodic identification $\theta \sim \theta + a$, where a is the circumference of the ring. We introduce a Gaussian source centered at $\theta = 0$,

$$J(t,\theta) = e^{-i\omega t}\frac{1}{\sqrt{8\pi\sigma^2}}\sum_n \exp\left(-\frac{(\theta-na)^2}{2\sigma^2 a^2}\right), \quad (1)$$

with the periodicity taken into account [16]. The source is coupled linearly to the physical field $O(t,\theta)$ defined on the ring [17]. The effect of the source propagates over the ring, and we measure the observable $O(t,\theta)$, to which we mathematically apply the Fourier optics to obtain the image. In the remainder of this section, we first introduce two models—a model for an ordinary material and another model for a spacetime-emergent material—for which in later sections we will check whether the above strategy works and then illustrate the physical meaning of the Fourier optics.

A. Ordinary material

In order to check whether our strategy really works, we prepare two models without and with the emergent spacetime. The first one is the free real scalar theory on the ring, with the source (1) added. The theory models scalar wave propagations in the simplest manner and is known to roughly approximate Nambu-Goldstone modes accompanying spontaneous symmetry breaking when the matter is gapless [18]. The action of the field $\phi(t,\theta)$, with the metric convention $\eta^{\mu\nu}=\mathrm{diag}(-1,1)$ and $\partial_\mu=(\partial_t,\partial_\theta)$, is given as

$$S_{\mathrm{nongrav}}=\int dtd\theta\left[-\frac{1}{2}\eta^{\mu\nu}\partial_\mu\phi(t,\theta)\partial_\nu\phi(t,\theta)-\frac{1}{2}m^2\phi(t,\theta)^2+J(t,\theta)\phi(t,\theta)\right], \tag{2}$$

whose equation of motion (EOM) is derived by the ϕ-variation:

$$(-\eta^{\mu\nu}\partial_\mu\partial_\nu+m^2)\phi(t,\theta)=J(t,\theta). \tag{3}$$

The model mimics the conductor-insulator transition characterized by the ratio of m to ω (but note that the carrier is now the boson ϕ). As we will later compute in Sec. III, the Green's function of (3) with frequency ω is given as

$$G(t,\theta)=\frac{1}{a}\sum_n\frac{e^{-i\omega t+ik_n\theta}}{k_n^2+m^2-\omega^2}\quad\left(k_n:=\frac{2\pi n}{a}\right). \tag{4}$$

From this we can see that it has resonance modes around $k_n^2\sim\omega^2-m^2$ when $m<\omega$, while no resonance is found when $m>\omega$, which is the reason for the transition.

B. Spacetime-emergent material

The second model is the simplest holographic CFT on the ring at nonzero temperature. "Holographic CFT" means that the CFT allows a bulk gravitational description under the AdS/CFT correspondence. Thus we describe this theory as an equivalent theory in the bulk. We consider, as the dual bulk gravity theory, a massless scalar field $\Phi(x^0,x^1,x^2)$ on a three-dimensional curved spacetime,

$$S_{\mathrm{grav}}=-\frac{1}{2}\int dx^3\sqrt{-g}\,g^{\mu\nu}\partial_\mu\Phi(x)\partial_\nu\Phi(x), \tag{5}$$

where x^μ ($\mu=0,1,2$) is the spacetime coordinate, ∂_μ is the x^μ derivative, $g_{\mu\nu}$ is the metric with norms of timelike vectors being negative, $g^{\mu\nu}$ is its inverse, and $g:=\det g_{\mu\nu}$. More specifically, the coordinates are $x^\mu=(t,\theta,r)$ with r being the radial coordinate (see Fig. 3). The radial coordinate is the emergent coordinate of the holographic spacetime.

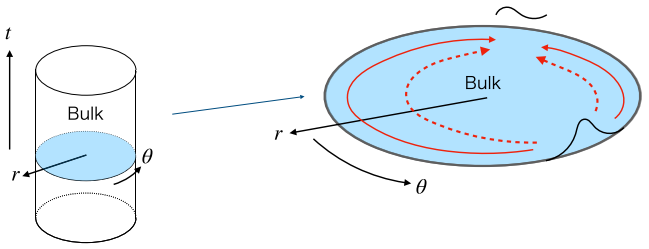

FIG. 3. The emergent spacetime dual to the holographic CFT. In the holographic material, the response to the source behaves as if the source perturbation had propagated inside the virtual curved spacetime, the bulk.

We adopt as $g_{\mu\nu}$ the following two kinds of spacetimes: the BTZ black hole spacetime and the AdS soliton spacetime [19]. The two spacetimes are solutions of the three-dimensional Einstein equation with a negative cosmological constant, and as explained in Sec. I there is a gravitational phase transition between them that is identified with the conductor-insulator transition on the material side. The BTZ black hole is favored when the temperature T is higher than $1/a$, and the AdS soliton is favored when T is lower than $1/a$.

In general, the explicit action of the holographic CFT is not available, while the duality tells us that the two spacetimes correspond to some different states in a certain CFT. According to the AdS/CFT dictionary, the bulk scalar field Φ corresponds to a composite operator $\hat{O}(t,\theta)$ in the CFT, whose expectation value $O(t,\theta)$ is now affected by the source J [given as (1)] linearly coupled to the operator $\hat{O}(t,\theta)$.

The dictionary to derive the expectation value from the calculations on the gravity side is as follows. The key tool connecting the bulk theory and the CFT is a dictionary called the Gubser-Klebanov-Polyakov-Witten (GKPW) relation [20,21]. First, we solve the EOM from (5),

$$\frac{1}{\sqrt{-g}}\partial_\mu(\sqrt{-g}g^{\mu\nu}\partial_\nu\Phi(x))=0, \tag{6}$$

to obtain the general solution. Here, the derivative operation acting on the bulk field Φ is the curved-spacetime version of the d'Alembertian. Then, we find that the solution asymptotically behaves as

$$\Phi(x)\sim A(t,\theta)+\frac{B(t,\theta)}{r^2} \tag{7}$$

near the boundary [22]. The dictionary [23] tells us to regard A and B as J and O, respectively.

Thus we adopt $A=J$ as one of the boundary conditions for our solution. We also have to put another boundary condition inside the bulk to fix the remaining arbitrary constant; we postpone considering it to Sec. III. From those two conditions, O is uniquely determined as a function of J, which is the response function we want [24].

C. Imaging transform

The method of Fourier optics realizes the visualization of the spacetime emergence. We apply the optical conversion

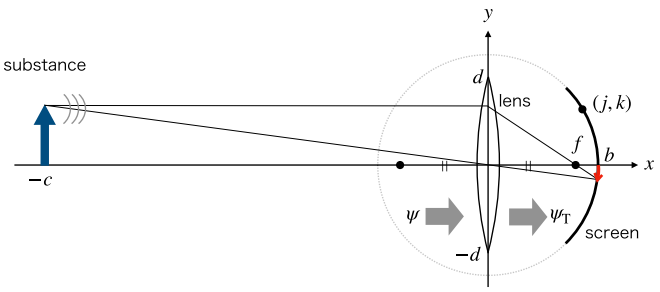

FIG. 4. The imaging by lens. The lens is located at $x = 0$, and the screen is at $x^2 + y^2 = b^2$, where f is the focal length. $2d$ is the length of the lens, c and b are the distances from the lens to the substance and from the lens to the screen, respectively. The thin lines represent the light orbits in the geometrical optics approximation.

formula just mathematically to the response function O, to visualize the bulk spacetime. Here we describe the mathematical formula, which is nothing but a Fourier transform.

To illustrate its physical meaning, let us first review how a substance is imaged by a convex lens and a screen as in Fig. 4. In the figure, spherical waves are emitted from points on the substance to reach the lens with the wave amplitude function being ψ, pass through the lens ($\psi_{\rm T}$), and then come to the screen ($\psi_{\rm S}$). The lens gives a phase to the transmitted wave: $\psi_{\rm T}(y) = e^{-iy^2/2f}\psi(y)$. The Huygens theorem says that the image at the screen is composed of the superposition of wavelets coming from the lens. Thus the wave at the screen is given as

$$\psi_{\rm S}(k) \propto \int_{-d}^{d} dy\, \psi_{\rm T}(y) \frac{e^{i\omega R(k,y)}}{R(k,y)}, \tag{8}$$

$$R(k,y) := \sqrt{j^2 + (k-y)^2}, \tag{9}$$

where (j, k) is the Cartesian coordinate on the screen, i.e., $j^2 + k^2 = b^2$.

We suppose $|y/b| \sim |k/b| \ll 1$, while ωy and ωk are kept $O(1)$. Then $\psi_{\rm S}$ is approximated as

$$\psi_{\rm S}(k) \propto \int_{-d}^{d} dy\, \psi(y) \exp\left[i\omega\left(\frac{y^2}{2c} - \frac{ky}{b}\right)\right], \tag{10}$$

where the formula of the lens, $1/f = 1/c + 1/b$, has been used. Even when the screen is put at $b = f$, the image may still not be so blurred if we take $c/f \gg 1$. In this case, we have

$$\psi_{\rm S}(k) \propto \int_{-d}^{d} dy\, \psi(y) e^{-i\omega k y/f}. \tag{11}$$

This is the mathematical imaging transform which is applied to the response function. The form is nothing but a Fourier transform.

Let us go back to our theory setup and apply the above formula to the response O as

$$\Psi(\theta_{\rm obs}; t, k) = \int_{\theta_{\rm obs}-d}^{\theta_{\rm obs}+d} d\theta\, e^{-i\omega\theta k/f} O(t,\theta). \tag{12}$$

In this expression, Ψ relates to O just as ψ does to $\psi_{\rm S}$; the convex lens is put at $\theta = \theta_{\rm obs}$ on the ring, with $y = \theta - \theta_{\rm obs}$ (as we have adopted the massless field in the bulk, the picture of the geometrical optics described above is still valid [25]). When the system has the emergent bulk spacetime, O will behave as if a wave had propagated there. In the picture of the geometrical optics, light rays are subject to the gravitational lens inside the bulk, which makes a virtual image for the observer at the boundary. The virtual image differs according to where the observer is located, and the lens functions as the observer's eyes. Thus Ψ contains geometric information about the bulk, which is why we claim that the imaging judges the spacetime emergence [26]. Actually, in higher-dimensional examples, the Einstein rings were visualized by using the same method [10–13]. When the system does not have any dual gravity system, on the other hand, the function Ψ does not allow any interpretation of the view of the bulk.

III. COMPUTATION OF RESPONSE FUNCTIONS

We compute the response function to the Gaussian source (1) for the two models introduced in Sec. II.

A. Ordinary material

Let us start with deriving the Green's function G introduced in (4), which satisfies

$$(-\eta^{\mu\nu}\partial_\mu\partial_\nu + m^2)G(t,\theta) = \sum_{n=-\infty}^{\infty} \delta(\theta - na), \tag{13}$$

where the right-hand side is the identity in the space of functions with period a. In experiments one expects dissipation, and the mode with the source frequency ω will dominate the response as the stationary state (while the equation above does not respect the dissipation). Thus we first use an ansatz $G(t,\theta) = e^{-i\omega t} g(\theta)$, to extract the dominant stationary part. By Fourier-expanding $g(\theta)$ and the right-hand side [k_n is defined in (4)],

$$g(\theta) = \frac{1}{\sqrt{a}} \sum_n g_n e^{ik_n\theta}, \tag{14}$$

$$\sum_n \delta(\theta - na) = \frac{1}{a}\sum_n e^{ik_n\theta}, \tag{15}$$

we obtain

$$g_n = \frac{1}{\sqrt{a}} \frac{1}{k_n^2 + m^2 - \omega^2},$$

i.e.,

$$g(\theta) = \frac{1}{a}\sum_n \frac{e^{ik_n\theta}}{k_n^2 + m^2 - \omega^2}. \tag{16}$$

From the Green's function, our solution of (3) is given as

$$\begin{aligned}\phi(t,\theta) &= e^{-i\omega t}\int_{-\infty}^{\infty} d\theta'\, g(\theta-\theta')J(\theta') \\ &= \frac{1}{2}\sum_n \frac{e^{-2\pi^2\sigma^2 n^2}}{k_n^2 + m^2 - \omega^2} e^{-i\omega t + ik_n\theta}.\end{aligned} \tag{17}$$

This is the response function in our non-SEM model.

B. Spacetime-emergent material

Here we compute the response function for our SEM model. There is the phase transition of the background between the BTZ black hole (the high-temperature phase, $T > 1/a$),

$$ds^2_{\rm BTZ} = -\frac{r^2 - r_h^2}{L^2}dt^2 + \frac{L^2}{r^2 - r_h^2}dr^2 + \frac{r^2}{L^2}d\theta^2, \tag{18}$$

and the AdS soliton (the low-temperature phase, $T < 1/a$),

$$ds^2_{\rm sol} = -\frac{r^2}{L^2}dt^2 + \frac{L^2}{r^2 - r_s^2}dr^2 + \frac{r^2 - r_s^2}{L^2}d\theta^2. \tag{19}$$

Here, L is the AdS radius, r_h is the horizon radius, and r_s is the gap of the AdS soliton. From the geometric regularity at $r = r_h$ and $r = r_s$ on the BTZ black hole and the AdS soliton, respectively, they are determined as

$$r_h = 2\pi L^2 T, \quad r_s = \frac{2\pi L^2}{a}. \tag{20}$$

For $a = 2\pi L$ ($r_s = L$), the AdS soliton is identical to the pure AdS in the global patch. Next, we compute the response function for each phase in order.

1. High-temperature phase

Let us first study the high-temperature phase, the BTZ phase. Since we are interested in the forced oscillation mode, we can expand the solution as

$$\Phi(x) = \sum_n \Phi_n(r) e^{-i\omega t + ik_n\theta}. \tag{21}$$

Putting

$$\Phi_n(r) = \xi^{-i\omega L^2/(2r_h)} f_n(\xi) \quad \left(\xi := 1 - \frac{r_h^2}{r^2}\right), \tag{22}$$

we obtain the simplified EOM,

$$\xi(1-\xi)f_n''(\xi) + \left(1 - \frac{i\omega L^2}{r_h^2}\right)(1-\xi)f_n'(\xi) - \left(\frac{L^4 n^2 \pi^2}{a^2 r_h^2} - \frac{L^4\omega^2}{4r_h^2}\right)f_n(\xi) = 0. \tag{23}$$

As this is the hypergeometric equation, the general solution around $\xi = 0$ ($r = r_h$) is written as

$$f_n(\xi) = C_n^1 F(\alpha_n, \beta_n, \gamma_n; \xi) + C_n^2 \xi^{1-\gamma_n} F(\alpha_n - \gamma_n + 1, \beta_n - \gamma_n, 2 - \gamma_n; \xi), \tag{24}$$

where F is the hypergeometric function and α_n, β_n, and γ_n are defined as

$$\alpha_n := -i\left(\frac{\omega L^2}{2r_h} + \frac{n\pi L^2}{a r_h}\right),$$
$$\beta_n := -i\left(\frac{\omega L^2}{2r_h} - \frac{n\pi L^2}{a r_h}\right),$$
$$\gamma_n := 1 + \alpha_n + \beta_n. \tag{25}$$

We determine the coefficients C_n^1 and C_n^2 by imposing the following two boundary conditions on the solution. First, we require the in-going boundary condition at the black hole horizon. In Φ_n given by (22) and (24), we have the near-horizon expression

$$e^{-i\omega t}\xi^{\mp i\omega L^2/(2r_h)} = \exp\left(-i\omega t \mp \frac{i\omega L^2}{2r_h}\ln\xi\right) \simeq \exp\left[-i\omega\left(t \pm \frac{L^2}{2r_h}\ln\frac{r - r_h}{r_h}\right)\right], \tag{26}$$

which leads us to impose $C_n^2 = 0$, i.e.,

$$\Phi(x) = \sum_{n=-\infty}^{\infty} C_n^1 e^{-i\omega t + ik_n\theta}\xi^{-i\omega L^2/(2r_h)} F(\alpha_n, \beta_n, \gamma_n; \xi). \tag{27}$$

The other condition is that the non-normalizable mode in the bulk corresponds to the source in the boundary theory, according to the AdS/CFT dictionary, as was explained in Sec. II. The asymptotic form of (27) near the boundary of the bulk $\xi \sim 1$ is, at the leading order,

$$\Phi(x) \sim \sum_{n=-\infty}^{\infty} C_n^1 e^{-i\omega t + ik_n\theta}. \tag{28}$$

By equating this to J of (1) (with $e^{-i\omega t}$ removed), we have

$$\sum_n C_n^1 e^{ik_n\theta} = \frac{1}{\sqrt{8\pi\sigma^2}}\sum_n \exp\left(-\frac{(x - na)^2}{2\sigma^2 a^2}\right). \tag{29}$$

Then the Fourier coefficient C_n^1 is determined as

$$C_n^1 \simeq \tfrac{1}{2}e^{-2\pi^2\sigma^2 n^2} \quad (\sigma \ll 1), \tag{30}$$

where we have replaced the integral domain $[-a/2, a/2]$ with $[-\infty, \infty]$ by supposing that the source is local.

Next, we read the response from the subleading term in the near-boundary expansion. By solving the asymptotic form of the EOM (6), one finds two modes r^0 and r^{-2}, as mentioned in Sec. II. The former is non-normalizable and corresponds to the source, while the latter is normalizable and corresponds to the response. Here we need to take care of a subtlety in the expansion: In fact, the correct expansion of (27) with (30) is, to $O(r^{-2})$, given as

$$\Phi(x) = \frac{1}{2}\sum_n e^{-i\omega t + 2ik_n\theta - 2\pi^2\sigma^2 n^2}\xi^{-i\omega L^2/(2r_h)} F(\alpha_n, \beta_n, \gamma_n; \xi) \sim \frac{1}{2}\sum_{n=-\infty}^{\infty} e^{-i\omega t + ik_n\theta - 2\pi^2\sigma^2 n^2} \times \left[1 + \frac{i\omega L^2 r_h}{2}\epsilon + r_h^2\alpha_n\beta_n\epsilon\ln\left(r_h^2\epsilon\right) + \alpha_n\beta_n\left(H_{\alpha_n} + H_{\beta_n} - 1\right)r_h^2\epsilon + O(\epsilon^2\ln\epsilon)\right], \tag{31}$$

where we have put $\epsilon := 1/r^2$ and H_p is the analytically continued harmonic number [27]. Then we find that the story seems more complex than we expected.

The problem is caused by the fact that the non-normalizable mode has $O(r^{-2}\ln r)$ and $O(r^{-2})$ terms as its next orders in solving the asymptotic EOM and they are more dominant than (as dominant as) the normalizable mode. If we

solve the asymptotic EOM to $O(r^{-2})$, the linear combination of the two modes reads

$$\sum_n e^{-i\omega t+ik_n\theta}\big[D_n^1\big(1+\alpha_n\beta_n r_h^2\epsilon\ln\big(r_h^2\epsilon\big)-(1+\alpha_n\beta_n)r_h^2\epsilon\big) + D_n^2\epsilon+O(\epsilon^2\ln\epsilon)\big]. \tag{32}$$

We can determine $D_n^{1,2}$ by comparing this with (31). The response can be read from the normalizable mode, the sum of the D_n^2 terms. Since we find that D_n^1 is identical to C_n^1 by construction, we obtain

$$D_n^2=\frac{r_h^2}{2}e^{-2\pi^2\sigma^2n^2}\left[1+\frac{i\omega L^2}{2r_h}+\alpha_n\beta_n\big(H_{\alpha_n}+H_{\beta_n}\big)\right], \tag{33}$$

and hence we conclude that the response function in the BTZ phase, the high-temperature phase ($T>1/a$), is

$$O_{\rm BTZ}(t,\theta)=\frac{r_h^2}{2}\sum_n\left[e^{-i\omega t+ik_n\theta-2\pi^2\sigma^2n^2}\times\left(1+\frac{i\omega L^2}{2r_h}+\alpha_n\beta_n\big(H_{\alpha_n}+H_{\beta_n}\big)\right)\right]. \tag{34}$$

2. Low-temperature phase

The computation in the low-temperature phase, the AdS soliton phase, is similar to the previous case. We obtain the same solution as (24), but with

$$\Phi_n(r)=\xi^{\pi|n|L^2/(ar_s)}f_n(\xi)\quad\left(\xi=1-\frac{r_s^2}{r^2}\right) \tag{35}$$

and

$$\alpha_n:=\frac{\pi|n|L^2}{ar_s}-\frac{\omega L^2}{2r_s},\quad \beta_n:=\frac{\pi|n|L^2}{ar_s}+\frac{\omega L^2}{2r_s},\quad \gamma_n:=1+\alpha_n+\beta_n \tag{36}$$

instead of (22) and (25), respectively.

As the boundary condition inside the bulk, in the previous AdS black hole case we considered the in-going boundary condition at the black hole horizon. Now, in the present AdS soliton geometry, the spacetime does not contain any black hole and is regular at $r=r_s$; so we require that Φ is not divergent at $r=r_s$. From this, we again get $C_n^2=0$. The response can be computed by following the same procedure as before. The response function in the AdS soliton phase, the low-temperature phase ($T<1/a$), is

$$O_{\rm sol}(t,\theta)=\frac{r_s^2}{2}\sum_n\left[e^{-i\omega t+ik_n\theta-2\pi^2\sigma^2n^2}\times\left(1-\frac{\pi|n|L^2}{2ar_s}+\alpha_n\beta_n\big(H_{\alpha_n}+H_{\beta_n}\big)\right)\right]. \tag{37}$$

Note that this $O_{\rm sol}$ does not have the T dependence.

IV. IMAGING RESPONSE FUNCTIONS

We apply the imaging transform (12) to ϕ in (17), $O_{\rm BTZ}$ in (34), and $O_{\rm sol}$ in (37). For the case of the SEM ($O_{\rm BTZ}$ and $O_{\rm sol}$), the physical meaning of the imaging transform can be understood with Fig. 4. The source J corresponds to the substance, Φ corresponds to the light rays, O corresponds to ψ, and Ψ corresponds to $\psi_{\rm S}$, with the lens put along the θ direction. (Also in the non-SEM case one can apply the imaging transform, but the resultant image will not allow any physical interpretation, because the non-SEM case does not let the radial direction emerge.) Note that since the imaging can be realized just by a mathematical operation, we do not need to bring the lens and screen for real. Since k always appears with f as k/f, we can set $f=1$. The result is as follows:

$$\Psi_\phi(\theta_{\rm obs};t,k)=\sum_n\frac{e^{-2\pi^2\sigma^2n^2}}{k_n^2+m^2-\omega^2}\times e^{i\theta_{\rm obs}(k_n-\omega k)}\frac{\sin\big(d(k_n-\omega k)\big)}{k_n-\omega k}, \tag{38}$$

$$\Psi_{\rm BTZ}(\theta_{\rm obs};t,k)=r_h^2\sum_n e^{-2\pi^2\sigma^2n^2}\underbrace{\left[1+\frac{i\omega L^2}{2r_h}+\alpha_n\beta_n\big(H_{\alpha_n}+H_{\beta_n}\big)\right]}_{\rm Eq.(25)}\times e^{i\theta_{\rm obs}(k_n-\omega k)}\frac{\sin\big(d(k_n-\omega k)\big)}{k_n-\omega k}, \tag{39}$$

$$\Psi_{\rm sol}(\theta_{\rm obs};t,k)=r_s^2\sum_n e^{-2\pi^2\sigma^2n^2}\underbrace{\left[1-\frac{\pi|n|L^2}{2ar_s}+\alpha_n\beta_n\big(H_{\alpha_n}+H_{\beta_n}\big)\right]}_{\rm Eq.(36)}\times e^{i\theta_{\rm obs}(k_n-\omega k)}\frac{\sin\big(d(k_n-\omega k)\big)}{k_n-\omega k}. \tag{40}$$

Recalling (20), we see that the AdS radius L contributes only as an overall factor; so we also set $L=1$.

Figure 5 shows a plot of each $|\Psi(\theta_{\rm obs};t,k)|^2$, which is no longer independent of t. We are able to identify the image of the low-temperature phase of the SEM (the AdS soliton phase) from the others, since its $\theta_{\rm obs}$ dependence of the response image is the most dramatic, while the others do not have such a strong dependence on $\theta_{\rm obs}$. For the AdS soliton, we catch a strong signal at $\theta_{\rm obs}=a/2$, while it cannot be seen at nonantipodal points ($\theta_{\rm obs}\neq a/2$), embodying the emergence of the bulk spacetime by "seeing" the source through the bulk [28]. In the high-temperature phase of the SEM (the BTZ phase), the image is hardly different from that of the non-SEM with large masses [29], and hence we need to explore the low-temperature phase in order to judge whether a spacetime is emergent.

Note that we need to tune the parameters as $2\pi/\omega\ll d\ll a$. The first inequality means that the lens size is much larger than the wavelength, which is necessary for the plots to have high resolution, and the second inequality guarantees that the plots include local information near $\theta_{\rm obs}$.

In Fig. 6, we show the density plots of Fig. 5, for the SEM model at low temperature (the AdS soliton case) and for the non-SEM model with $m=55\pi/a$. For the AdS soliton, the image is bright only at the antipodal point, while for the non-SEM model the images get brighter when the observation point $\theta_{\rm obs}$ approaches the source.

The behavior of the response image of the SEM model allows in fact the geometric interpretation of the emergent

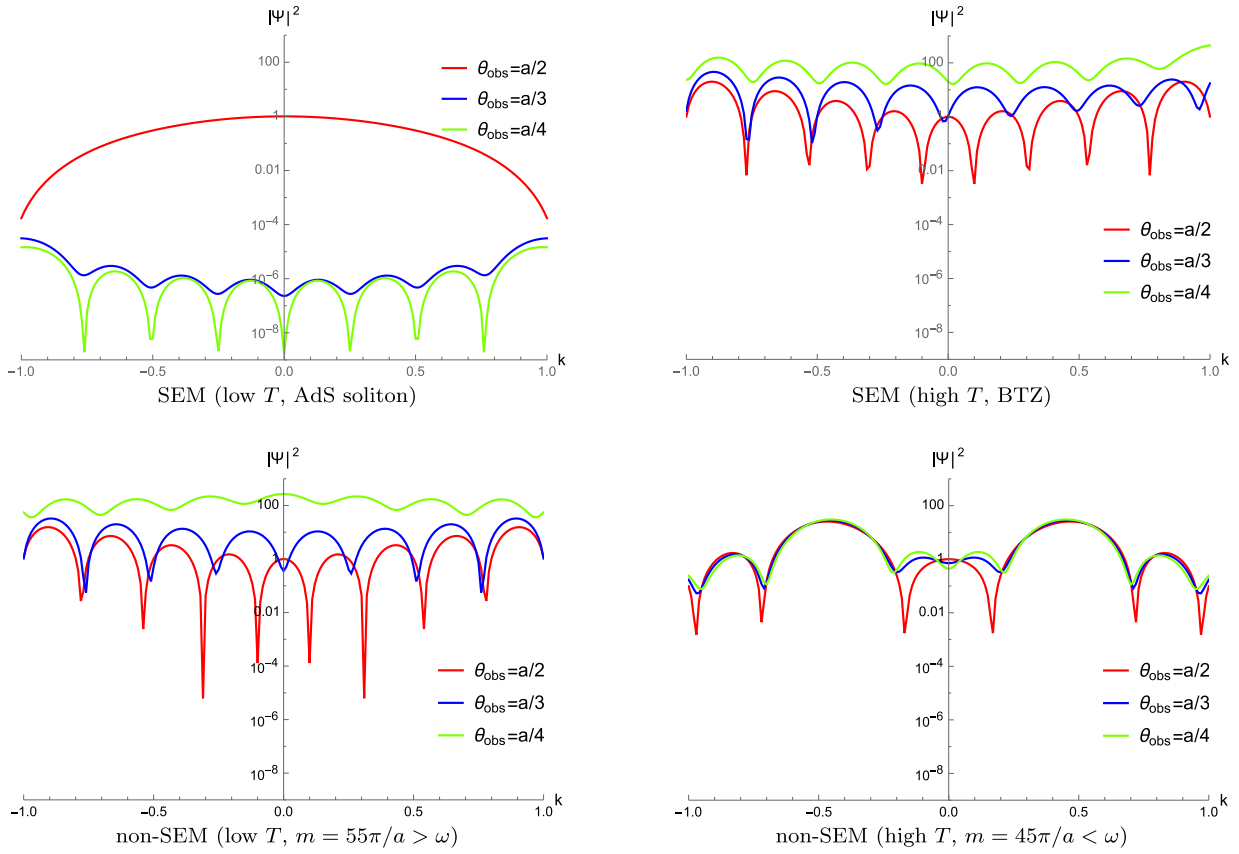

FIG. 5. Plots of the images of the response functions. The upper row is for SEM, and the lower row is for non-SEM. On the other hand, the left column is for the low-temperature phase, and the right column is for the high-temperature phase (though the non-SEM model does not depend on temperature, the transition due to the ratio m/ω mimics the conductor-insulator transition, which is usually determined by temperature). The three plots in each panel are normalized so that the plot function for $\theta_{\rm obs} = a/2$ at $\theta = 0$ is set to be 1. Parameters, except $\sigma = 10^{-2}$ (the width of J is $a\sigma$), are chosen so that a determines their dimension: $\omega = 101\pi/(2a)$, $d = a/(4\pi)$, and the others are shown above. Because of this choice, a contributes to Ψ only as its overall factor; thus we can set a arbitrarily. For Ψ to have local information, d should be sufficiently smaller than a, but at the same time, it should be larger than the wavelength, $2\pi/\omega$, to keep the resolution of the images.

spacetime. Let us consider the geometrical optics approximation (the geodesic analysis). From (18) and (19), null geodesics shot from the boundary point are given as

$$\begin{aligned}
\text{BTZ:}\quad t(\lambda) &= \frac{1}{r_h}\coth^{-1}\left(\frac{(1-l^2)\lambda}{r_h}\right),\\
\theta(\lambda) &= \frac{1}{r_h}\coth^{-1}\left(\frac{(1-l^2)\lambda}{l r_h}\right),\\
r(\lambda) &= \sqrt{(1-l^2)\lambda^2 - \frac{r_h^2 l^2}{1-l^2}} \qquad (41)\\
\text{AdS soliton:}\quad t(\lambda) &= \frac{1}{r_s}\tan^{-1}\left(\frac{(1-l^2)\lambda}{r_s}\right) + \frac{\pi}{2r_s},\\
\theta(\lambda) &= \frac{1}{r_s}\tan^{-1}\left(\frac{(1-l^2)\lambda}{l r_s}\right) + \frac{\pi}{2r_s},\\
r(\lambda) &= \sqrt{(1-l^2)\lambda^2 + \frac{r_s^2}{1-l^2}}, \qquad (42)
\end{aligned}$$

respectively, where $l \in (-1, 1)$ is the parameter classifying null geodesics and λ is the world-line coordinate which, when eliminated through $(t(\lambda), \theta(\lambda), r(\lambda))$, provides the bulk geodesic $\theta(r)$. Each geodesic starts at $(t, \theta, r) = (0, 0, \infty)$, where $\lambda = -\infty$. The two geodesic families are shown in Fig. 7. In the BTZ spacetime, all light rays go down into the horizon and never come back to the boundary. In the AdS soliton spacetime, on the other hand, all light rays are accumulated to reach the antipodal point, vertically to the boundary line due to the gravitational lens; in the AdS soliton case, $d\theta/dr \to 0$ as $\lambda \to \pm\infty$. The image view consists of a bright spot of light coming from the front. Thus in this sense, we can say that the imaging transform visualizes the spacetime emergence [30].

V. MATERIAL PARAMETERS FOR SEARCH EXPERIMENT

As we have emphasized in the Introduction, ring-shaped materials are suitable in searching for spacetime-emergent materials. Here in this section we look at the parameters of the theory toward the experimental realization. The parameters are the circumference of the ring a, the angular frequency of the source ω, and the temperature T. The realization highly depends on the actual values of these parameters and, in particular, depends on what kind of waves we consider on the

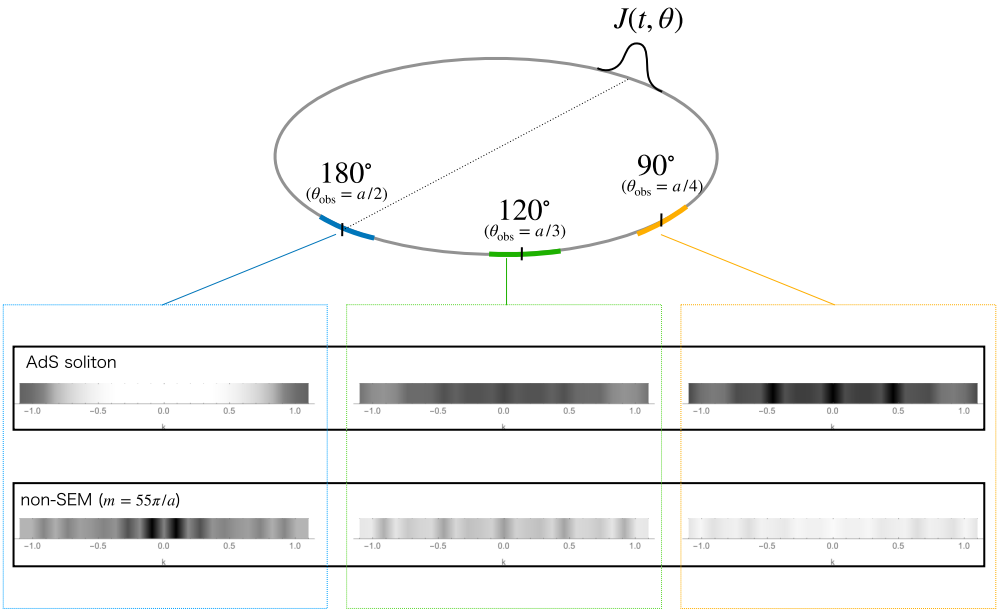

FIG. 6. Density plots of the images of the response functions at $\theta_{obs} = a/2$, $a/3$, and $a/4$. The upper row is for the SEM model at the low-temperature phase (AdS soliton), and we plot a function $(4 + \log_{10}|\Psi|^2)/7$ which roughly ranges from 0 to 1 for the computed image values. The lower row is for the non-SEM model (with the scalar mass $n = 55\pi/a$), where we plot $(12 + \log_{10}|\Psi|^2)/7$, which again roughly ranges from 0 to 1.

materials. Below we explicitly propose $TlCuCl_3$ for the material and calculate the values of the parameters for possible experiments.

Among the quantum critical points (QCPs) observed and proposed in the literature, one of the suitable QCPs for our purpose is that related to spin waves (magnons) [31]. In this case, the observable operator $\mathcal{O}$ is the spin density operator, and J, the source linearly coupled to $\mathcal{O}$, could be the electromagnetic source. In the actual experiment, the Fourier optics imaging can be performed numerically from data sets of $\mathcal{O}(\theta)$.

There are various reasons for choosing the spin wave, as listed below.

(i) The waves conduct only on the ring and do not propagate in the physical space inside of the ring. If we had used electromagnetic waves instead of spin waves, they would have propagated inside the ring, and the holographic emergence could not have been checked.

(ii) We can get closer to the QCP. If we had instead used a high-T_c superconductor, commonly studied in the field of AdS/CMP correspondence, the QCP would have been hidden inside the superconducting dome in the parameter space.

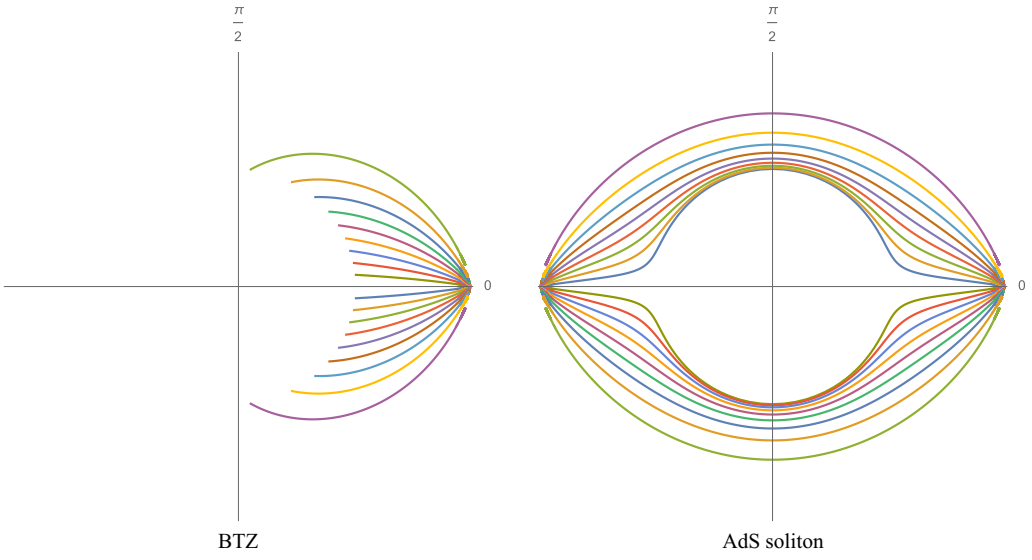

FIG. 7. Null geodesics shot from a boundary point, projected onto the (r, θ) plane. The two axis labels indicate the value of $2\pi\theta/a$ in those directions. In these diagrams the radial direction is scaled to show the spatial boundary $r = \infty$ at a finite range, by a new radial coordinate $(2/\pi)\tan^{-1} r$. The null geodesics in the BTZ spacetime reach the black hole horizon at $\lambda = -r_h/(1 - l^2)$.

(iii) We can use electrical insulators. If we had used conducting materials, the electromagnetic waves used for controlling the source would also have affected the conduction itself.

(iv) The coherence length for spin waves can be long enough so that the continuum approximation of our theory can be justified.

For these reasons, we come to consider thallium copper chloride, $TlCuCl_3$. It is one of the popular materials that exhibit the quantum phase transition, which can be controlled not by the material compositions but by the external magnetic field or pressure [32,33] (see also a review article [34] which mentions the material and the application to the holographic principle). Below, we use material parameters of $TlCuCl_3$ to check whether the consistency conditions of our theory setup are satisfied or not, to see the experimental realization.

Our theory, in particular the analyses of the AdS soliton geometry, needs the following two conditions. First, the imaging condition

$$\omega \gg \frac{2\pi v}{a} \tag{43}$$

is required so that the imaging resolution is high. This condition means that the wavelength on the ring material is small compared with the size of the lens region. Here we have restored v, which is the speed of the wave propagation on the ring [35]. Second, we require the low-temperature condition

$$\frac{v\hbar}{a} > k_{\rm B}T, \tag{44}$$

since we are going to probe the AdS soliton geometry which is realized at low temperature. The threshold is located at the phase-transition temperature separating the soliton phase from the BTZ black hole phase, $T = 1/a$ in units of $v = \hbar = k_{\rm B} = 1$. These two conditions (43) and (44) are the necessary conditions for the theory analyses to be valid.

Let us substitute material values for these conditions. With the velocity of the magnon on the material $TlCuCl_3$ estimated roughly as $v \simeq 2 \times 10^3$ m/s [36], we consider the following three cases for the temperature value for the SEM search experiment.

(*i*) $T \simeq 1.5$ K. This is the value considered in Refs. [32,33]. From (44) we get $a \lesssim 10$ nm, which is so small that the lattice effect of the material cannot be ignored, since the lattice constant [37] of $TlCuCl_3$ is about 1 nm. For this maximum value $a \sim 10$ nm, the condition (43) gives the frequency $\nu \equiv \omega/2\pi \gg 10^2$ GHz, and special experimental care may be necessary to prepare the source.

(*ii*) $T \simeq 10$ K. From (44) we get $a \lesssim 1$ nm, which is too small for the continuum theory to be valid.

(*iii*) $T \simeq 0.1$ K. From (44) we get $a \lesssim 10^2$ nm. This is much larger than the lattice constant of the material; thus our continuum limit is justified. The condition (43) gives the frequency $\nu \equiv \omega/2\pi \gg 10$ GHz. This value is accessible for the source to be prepared by the electromagnetic method.

A general relation found here is summarized as follows. For temperature $T \sim 10^n$ K, the ring circumference needs to satisfy $a \lesssim 10^{1-n}$ nm, and the frequency ν of the source needs to satisfy $\nu \gg 10^{n+2}$ GHz. Therefore the material parameters for our theory analyses to be valid allow a small window: $n \lesssim -1$.

These rough calculations show that the theory conditions (43) and (44) are satisfied in low-temperature experiments, providing a realistic possibility for the experimental search for spacetime-emergent materials.

VI. SUMMARY AND DISCUSSION

In this paper, we have provided a theoretical basis for future experiments searching for spacetime-emergent materials (SEMs). When a local source is put at a point on the ring-shaped material, the response function behaves differently according to whether or not the material of interest is an SEM. The difference is manifested by the visualization using the imaging transform of the response. The most distinguishable feature is that for the case of the SEM, the image shows a strong signal at the antipodal point of the ring when the material is cooled enough. This feature in fact allows the geometric interpretation of the emergent spacetime, since in our calculated examples the image coincides with the expectation from the geometrical optics approximation in the bulk (geodesic analysis). Thus we claim that this imaging method with the ring-shaped material prepared can verify the spacetime emergence.

The imaging method extracts geometric information from the response data, because it provides the image as if the observer looks into the holographically emergent curved spacetime. Null rays emitted from the source propagate on the curved geometry and reach points on the boundary. When the geometry is flat, the image transformation shoots an image of the same figure as the source, but when not, it usually shoots a virtual image created by the so-called gravitational lens. Thus the virtual image provided by the imaging transform is far more convincing than the raw data of the response, from the viewpoint of checking the spacetime emergence. A possible criticism is that the response function itself may be enough as a signal (see Fig. 8). However, we can argue that the transformed plot for the AdS soliton has no node and will be more robust against noise than the raw plot (the noise effect would depend on the details of the experimental setup). In addition, our AdS soliton can be technically distinct, as it allows the unique behavior that all null geodesics reach at the antipodal point. Therefore the imaging transform will be more valuable for surveying geometries different from the AdS soliton [38].

We have also discussed possible directions for realizing our strategy in laboratories, proposing a candidate SEM. The material $TlCuCl_3$, which has a quantum critical point at zero temperature, allows us to have enough material information including the magnon speed and lattice structure. This has enabled us to estimate experimental parameters for the search for SEMs; for example, at the temperature $T = 0.1$ K the source frequency needs to be a lot larger than 10 GHz, and the ring radius needs to be smaller than 10^2 nm. These values are realizable in future experiments.

Note that our discovery method actually utilizes the limitation of the conformal invariance. At the quantum critical point, the theory is scale-free and so is expected to be conformally invariant. At zero temperature, the two-point function (Green's function) of the CFT on a ring is completely determined by the conformal invariance with the dimensions of the operator, and thus the response to the source to the first

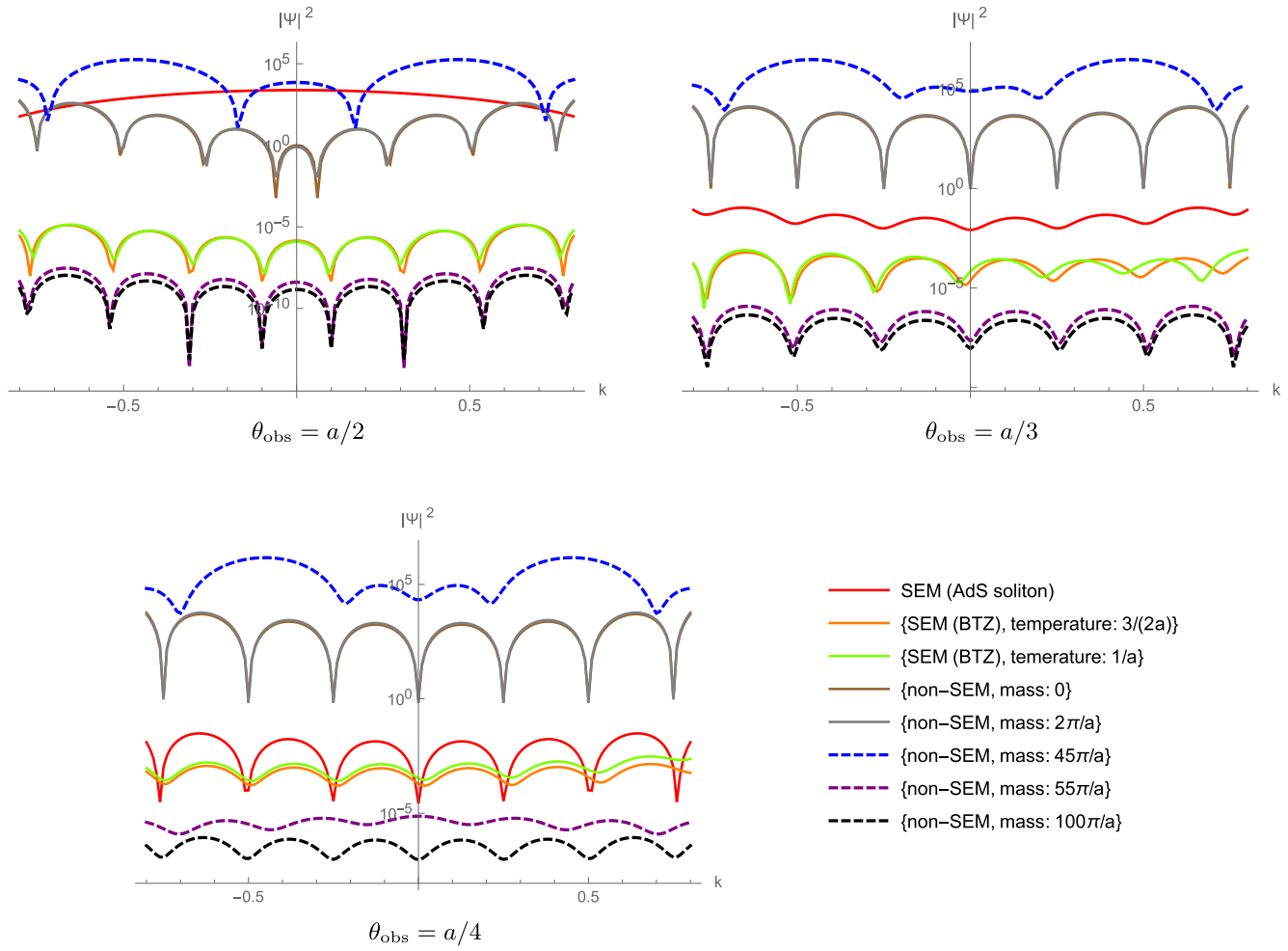

FIG. 8. Plots of the images of the response functions.

order is also determined from the symmetry; there is no room for the peculiarity of the SEM as opposed to the non-SEM to appear. However, when this CFT on a ring is put at a nonzero temperature, the conformal symmetry is reduced and cannot determine the correlator completely [39], where the difference between the SEM and the non-SEM appears. Only the SEM keeps the zero-temperature correlator intact in $T < 1/a$, while the non-SEM correlator largely depends on temperature and is characterized by the thermal free correlator. It is an interesting observation that our discovery channel actually is owing to the fact that experiments cannot reach the exact zero temperature; at zero temperature any system is just dictated by the whole conformal symmetry, and the SEMs are not clearly distinguishable.

Finally, let us argue for the universality of the SEM model we have adopted in this paper. Our SEM model is the simplest choice, a bulk massless scalar field theory on the two different background geometries, the BTZ black hole and the AdS soliton. Here, we present some arguments for the universality of our results in the presence of the following typical modifications and generalizations of the SEM theory.

(*i*) *Addition of other fields and different spins.* When there are several orders in the material, or there are orders associated with global symmetries or magnetization, it is natural to expect that several operators with different spins are involved in theoretical realization of the ring-shaped material. In the AdS/CFT dictionary, those situations correspond to having several bulk fields with different spins. Will these changes affect our theoretical results? First, our geometrical optics approximation works well while it is applied to massless higher-spin fields. Second, our calculation of the response function is robust against the addition of scalar fields, because it needs only Green's functions on the ring or in the bulk. Even when there are several fields, one can diagonalize the Hamiltonian and apply the Green's function method for each diagonalized component. Therefore we expect that our basic strategy works for any model with small field amplitudes, and our results are robust.

(*ii*) *Change in the mass of the field.* One can generalize the SEM model by adding a mass to the bulk field. According to the AdS/CFT dictionary it changes the scaling dimension of the boundary operator O that couples to the source. The masslessness of the field is nothing special, since the mass squared of the bulk field can be negative and just needs to be larger than or equal to the Breitenlohner-Freedman bound. Thus it is expected that the change in the mass of the bulk field will not give any drastic change in our result. Additionally, high-energy modes tend to be dominant in boundary-to-boundary propagators, and the mass can effectively be ignored. Thus we can expect that similar results will appear in massive cases.

Also note that, as (12) is just a mathematical operation (a class of finite Fourier transforms), it can also be applied formally to any O, not limited to light waves.

(*iii*) *Deformation of the background curved geometries.* The low-temperature phase of our SEM is described by the AdS soliton geometry. Although this geometry is ensured by the conformal symmetry under the holographic principle and thus does not allow any deformation [40], realistic experiments may not be performed exactly on the quantum critical point, and this may lead to possible deformations of the AdS soliton geometry. In particular, our discovery scheme of SEMs is owing strongly to the fact that all null geodesics focus on the unique antipodal point on the ring, which will not be exact in the deformed spacetimes. However, null geodesics should still be focused near the antipodal point, and hence there will remain the fundamental feature that the image at the antipodal point is far stronger than those at different points. Another issue is the interference of waves. When the focus of null geodesics is blurred due to the change in the geometry, the image at the antipodal point in the low-temperature phase may acquire nodes due to the interference, while there is no node in the image of the exact AdS soliton case. The nodal image would be similar to that of the non-SEM model with $m \lesssim \omega$, such as $m = 45\pi/a$ in Fig. 5, and hence it could falsify our discrimination method of the emergent spacetime. However, we can argue that the $\theta_{\rm obs}$ dependence of the image cures our method. It is seen in Fig. 5 that the magnitude of the image of $m = 45\pi/a$ does not vary so much when we change the value of $\theta_{\rm obs}$. On the other hand, even when the AdS soliton is deformed, the image in the low-temperature phase will vary significantly in $\theta_{\rm obs}$, because null geodesics do not reach boundary points not near the antipodal point, as described above. Therefore we expect that our method is sustainable against the continuous deformation of the background geometry of the emergent spacetime.

With these expectations, we hope that experiments are performed in the near future to find a spacetime-emergent material for quantum gravity experiments.

ACKNOWLEDGMENTS

We would like to thank Yoichi Yanase for valuable advice and Keiju Murata for discussions. The work of K.H. is supported in part by JSPS KAKENHI Grants No. JP22H05115, No. JP22H05111, and No. JP22H01217. The work of D.T. is supported by Grant-in-Aid for JSPS Fellows No. 22J20722. The work of K.T. is supported by MEXT Q-LEAP (Grant No. JPMXS0118067634) and by JSPS Grant-in-Aid for Scientific Research (S) (Grant No. JP21H05017). The work of S.Y. is supported in part by JSPS KAKENHI Grants No. 22H04473 and No. 22H01168.

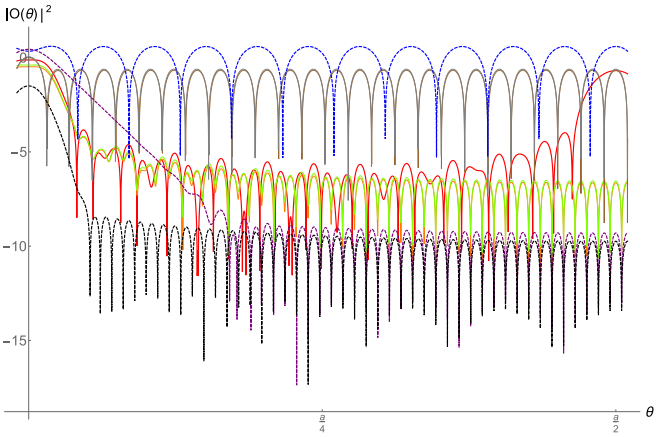

FIG. 9. Response functions. The legend in Fig. 8 applies here as well (the AdS soliton case is shown by the red line).

APPENDIX: PLOT OF RESPONSE FUNCTIONS

In this Appendix, we show details of the response functions and the images. First, in Fig. 8 we present detailed images for various non-SEM and SEM models. Since we did not care about the overall factors, we cannot compare the magnitude difference between the two models (comparison of relative magnitude within the same model is still accurate).

We also present a plot of the response functions which are to be Fourier transformed, for readers' reference. See Fig. 9. The legend in Fig. 8 applies to Fig. 9 as well. The relative overall normalization between the two models should not be trusted, as was explained above.

Among the plots, the response function of the AdS soliton case (which is the SEM case at the low-temperature phase) exhibits the unique feature that the amplitude of the response function grows by several orders at the antipodal point of the ring. This feature is consistent with our imaging [41].

[1] J. M. Maldacena, The large N limit of superconformal field theories and supergravity, Adv. Theor. Math. Phys. **2**, 231 (1998).

[2] A. Pelat, F. Gautier, S. C. Conlon, and F. Semperlotti, The acoustic black hole: A review of theory and applications, J. Sound Vib. **476**, 115316 (2020).

[3] A. A. Soluyanov, D. Gresch, Z. Wang, Q. Wu, M. Troyer, X. Dai, and B. A. Bernevig, Type-II Weyl semimetals, Nature (London) **527**, 495 (2015).

[4] The subscripts denote their spacetime dimensions. A short introduction to the AdS/CFT correspondence will be given later in this section.

[5] When $d = 2$, the sphere is a ring. We call this CFT$_d$ because the spacetime is a d-dimensional $\mathbb{R} \times \mathbb{S}^{d-1}$, where $\mathbb{R}$ denotes the time coordinate.

[6] A. Karch and A. O'Bannon, Metallic AdS/CFT, J. High Energy Phys. 09 (2007) 024.

[7] S. A. Hartnoll, C. P. Herzog, and G. T. Horowitz, Building a Holographic Superconductor, Phys. Rev. Lett. **101**, 031601 (2008).

[8] S. A. Hartnoll, C. P. Herzog, and G. T. Horowitz, Holographic superconductors, J. High Energy Phys. 12 (2008) 015.

[9] In constructing holographic CMP models, one may also think of comparing the theoretical spectra with experiments; however,

such a bottom-up construction of the gravity model having the same spectrum is almost equivalent to finding a new AdS/CFT example, and so it is definitely a difficult problem.

[10] K. Hashimoto, S. Kinoshita, and K. Murata, Imaging black holes through the AdS/CFT correspondence, Phys. Rev. D **101**, 066018 (2020).

[11] K. Hashimoto, S. Kinoshita, and K. Murata, Einstein Rings in Holography, Phys. Rev. Lett. **123**, 031602 (2019).

[12] Y. Kaku, K. Murata, and J. Tsujimura, Observing black holes through superconductors, J. High Energy Phys. 09 (2021) 138.

[13] Y. Liu, Q. Chen, X.-X. Zeng, H. B. Zhang, W.-L. Zhang, and W. Zhang, Holographic Einstein ring of a charged AdS black hole, J. High Energy Phys. 10 (2022) 189.

[14] The CFT is a scale-free theory and thus has no phase-transition scale. The only scale of this CFT on the ring is the ring circumference a. Therefore the phase transition occurs at the temperature $T = 1/a$. This rather peculiar transition temperature of the SEM is in contrast to the ordinary phase transition in materials.

[15] Although there may be a variety of possible modified SEM models, the feature is physically so firm that we expect they should still exhibit the feature, as discussed in Sec. VI.

[16] The normalization factor is chosen to simplify later expressions. We have assumed the relativity and have set the material "speed of light" to unity. We have also assumed the isotropy of the material for simplicity, so that the speed of light does not depend on the direction of the propagation.

[17] The corresponding experimental descriptions are found in Sec. V.

[18] We would like to thank Youichi Yanase for valuable advice on this point.

[19] In computing the response for Φ we keep the geometry $g_{\mu\nu}$ fixed (nondynamical). This is called probe approximation, and it is justified since the source magnitude is supposed to be very small so as not to alter the temperature of the whole system; thus the back reaction of the scalar field to the gravity field is ignored.

[20] S. S. Gubser, I. R. Klebanov, and A. M. Polyakov, Gauge theory correlators from noncritical string theory, Phys. Lett. B **428**, 105 (1998).

[21] E. Witten, Anti-de Sitter space and holography, Adv. Theor. Math. Phys. **2**, 253 (1998).

[22] As we will see later in the detailed computation, this is not the precise expression in our setup though valid in most cases.

[23] I. R. Klebanov and E. Witten, AdS/CFT correspondence and symmetry breaking, Nucl. Phys. B **556**, 89 (1999).

[24] Strictly speaking, the overall factor of O is in general different from B. However, we are interested not in the overall factor, which will depend on the details of the material, but only in the form of the function (the shape in its plot).

[25] We will discuss the case when the field is massive in Sec. VI.

[26] Since the proper distance along the radial direction from a boundary point to a bulk point is always divergent, the condition $c/f \gg 1$ is automatically satisfied.

[27] H_p is related to the digamma function $\psi(p)$ as $H_p = \gamma + \psi(p+1)$, where γ is the Euler's constant.

[28] The peculiarity of the AdS soliton phase with the strong signal can be seen also in the response function itself. See the Appendix for an explicit plot of the response functions.

[29] Note that the magnitude of the image function for the non-SEM model shows the ordinary expected transition from the conducting phase to the insulator phase when the temperature is lowered (or, equivalently, the mass m is increased against ω).

[30] In experiments with real materials, the emergent geometry may not exactly be the AdS soliton geometry; it could be some deformed geometry. We will discuss this issue in Sec. VI.

[31] The rigidity of our result in the presence of change in the carrier's spin is discussed in Sec. VI.

[32] M. Matsumoto, B. Normand, T. M. Rice, and M. Sigrist, Magnon Dispersion in the Field-Induced Magnetically Ordered Phase of $TlCuCl_3$, Phys. Rev. Lett. **89**, 077203 (2002).

[33] M. Matsumoto, B. Normand, T. M. Rice, and M. Sigrist, Field- and pressure-induced magnetic quantum phase transitions in $TlCuCl_3$, Phys. Rev. B **69**, 054423 (2004).

[34] S. Sachdev and B. Keimer, Quantum criticality, Phys. Today **64**(2), 29 (2011).

[35] In the theoretical analyses in previous sections we have put $v = 1$ as it corresponds to the speed of light, following high-energy theory notations. For numerical simulations, we took $\omega = 101\pi v/(2a) \gg 2\pi v/a$.

[36] The magnon speed v can be estimated as follows. According to the measured dispersion relation described in Fig. 2 of Ref. [42], at the near-gapless point $C = (0, 0, 1)$ in the reciprocal space, the slope of the dispersion is evaluated as 2.1 meV Å for the $(1, 0, -2)$ direction, 12 meV Å along the b^* axis, and 21 meV Å along the c^* axis, respectively. These slopes correspond to the propagation speeds of 3.1×10^2, 1.8×10^3, and 3.3×10^3 m/s, respectively. Thus if the ring is made from a flake whose in-plane directions are away from the $(1, 0, -2)$ direction (i.e., the direction with the slowest magnon velocity), the magnon dispersion can be reasonably isotropic in the ring plane of the material. This can be done, for example, by cleaving the material along the $(1, 0, -2)$ plane, which is one of the cleavage planes. Then, the propagation speed in the ring is rather isotropic with the value around $v \sim 2 \times 10^3$ m/s. We use this value for the evaluation of the experiment parameters.

[37] According to Ref. [43], the lattice parameters of $TlCuCl_3$ at room temperature are $b = 14.1440$ Å and $c = 8.8904$ Å.

[38] We plan to study a bulk reconstruction of the geometry from the response data, by using deep learning [44,45]. The imaging will also help in constructing the architecture of the neural networks, as the geodesic directly probes the spacetime which is identified as the neural network.

[39] For the determination of the retarded Green's function of any CFT on a line at nonzero temperature and its coincidence with the holographic gravity calculation, see Ref. [46]. In general, when the system is put on a ring at nonzero temperature, the CFT partition function is a torus partition function which is not determined completely by the conformal invariance only. So the two-point functions which we study in this paper are not determined either.

[40] In the AdS/CFT correspondence, the CFT_2 on $\mathbb{R}^{1,1}$ in the ground state corresponds to the pure Poincaré AdS_3. This is because the conformal symmetry of the CFT_2 is SO(2,2), which is the isometry of the bulk geometry. Now, when the CFT_2 is put on a compactified ring, the conformal symmetry is $SO(2,2)/\Gamma$, where Γ is the discrete spatial translation by the circumference a. On the gravity side, $SO(2,2)/\Gamma$ still guarantees the same number of Killing vectors as that of maximally symmetric spacetimes, and hence the geometry must be locally AdS_3.

There are two possible spacetimes which possess SO(2,2)/Γ; one is the AdS soliton, which we considered, and the other is obtained simply by compactifying the Poincaré AdS_3 with Γ. Only the former spacetime holographically reproduces the entanglement entropy of the CFT_2 on $\mathbb{R}^1 \times \mathbb{S}^1$, and the one which is favored from the viewpoint of the free energy computed from the Euclidean Einstein gravity is also the former. Therefore this symmetry argument singles out only the AdS soliton geometry as the gravitational dual of the CFT_2 on the ring.

[41] Note that the imaging was necessary to probe the bulk geometry directly, because the response function itself is subject to phase interference which needs to be decoded by the Fourier transform.

[42] N. Cavadini, G. Heigold, W. Henggeler, A. Furrer, H.-U. Güdel, K. Krämer, and H. Mutka, Magnetic excitations in the quantum spin system $TlCuCl_3$, Phys. Rev. B **63**, 172414 (2001).

[43] H. Tanaka, A. Oosawa, T. Kato, H. Uekusa, Y. Ohashi, K. Kakurai, and A. Hoser, Observation of field-induced transverse Néel ordering in the spin gap system $TlCuCl_3$, J. Phys. Soc. Jpn. **70**, 939 (2001).

[44] K. Hashimoto, S. Sugishita, A. Tanaka, and A. Tomiya, Deep learning and the AdS/CFT correspondence, Phys. Rev. D **98**, 046019 (2018).

[45] K. Hashimoto, S. Sugishita, A. Tanaka, and A. Tomiya, Deep learning and holographic QCD, Phys. Rev. D **98**, 106014 (2018).

[46] D. T. Son and A. O. Starinets, Minkowski space correlators in AdS/CFT correspondence: Recipe and applications, J. High Energy Phys. 09 (2002) 042.